THE JOURNAL OF BIOLOGICAL CHEMISTRY VOL. 292, NO. 8, pp. 3299–3311, February 24, 2017

Characterization of the Ruler Protein Interaction Interface on the Substrate Specificity Switch Protein in the *Yersinia* Type III Secretion System*[S]

Received for publication, November 29, 2016, and in revised form, December 29, 2016 Published, JBC Papers in Press, December 30, 2016, DOI 10.1074/jbc.M116.770255

Oanh Ho[‡], Per Rogne[‡], Tomas Edgren[§], Hans Wolf-Watz[§], Frédéric H. Login[§1], and Magnus Wolf-Watz[‡2]

From the [‡]Department of Chemistry, Chemical Biological Centre and [§]Department of Molecular Biology and The Laboratory for Molecular Infection Medicine Sweden (MIMS), Umeå University, S-901 87 Umeå, Sweden

Edited by Thomas Söllner

Many pathogenic Gram-negative bacteria use the type III secretion system (T3SS) to deliver effector proteins into eukaryotic host cells. In *Yersinia*, the switch to secretion of effector proteins is induced first after intimate contact between the bacterium and its eukaryotic target cell has been established, and the T3SS proteins YscP and YscU play a central role in this process. Here we identify the molecular details of the YscP binding site on YscU by means of nuclear magnetic resonance (NMR) spectroscopy. The binding interface is centered on the C-terminal domain of YscU. Disrupting the YscU-YscP interaction by introducing point mutations at the interaction interface significantly reduced the secretion of effector proteins and HeLa cell cytotoxicity. Interestingly, the binding of YscP to the slowly self-cleaving YscU variant P264A conferred significant protection against autoproteolysis. The YscP-mediated inhibition of YscU autoproteolysis suggests that the cleavage event may act as a timing switch in the regulation of early *versus* late T3SS substrates. We also show that $YscU_C$ binds to the inner rod protein YscI with a dissociation constant (K_d) of 3.8 μM and with 1:1 stoichiometry. The significant similarity among different members of the YscU, YscP, and YscI families suggests that the protein-protein interactions discussed in this study are also relevant for other T3SS-containing Gram-negative bacteria.

Yersinia spp. share a common virulence plasmid that encodes a type III secretion system (T3SS)[3] supporting the secretion of the *Yersinia* outer protein (Yop) effectors from the bacterium into eukaryotic host cells (1). After translocation into the host cells, Yop effectors counteract immune defense mechanisms such as phagocytosis or apoptosis and thereby promote the survival and propagation of the extracellular bacteria (2). Many pathogenic and symbiotic Gram-negative bacteria also utilize the T3SS to deliver proteins during the interactions with their hosts (3, 4). The T3SS (also referred to in the literature as the non-flagellar T3SS) evolved from the flagellum, and both systems present a similar architecture (5, 6) featuring a basal body assembly consisting of a multiringed complex that spans the bacterial envelope (5). However, the basal body of the flagellum is connected to an extracellular hook that forms a link with the flagellar filament. In contrast, the T3SS basal body is attached to a needle (in animal pathogens) or a pilus (in plant pathogens) that protrudes from the bacterial surface (5, 7, 8). The basal body and the needle/pilus together form the so-called needle complex that is the hallmark of the T3SS.

It is accepted that the needle complex is assembled in a stepwise manner, and in *Yersinia* spp., it has been shown that the inner membrane platform (formed by YscR, -S, -T, -U, and -V) is assembled independently of the outer membrane ring-forming proteins (YscC, -J, and -D) (9). After association of the inner and outer rings (mediated by YscJ), the secretion of the so-called early substrates such as the needle subunit YscF begins, which results in elongation of the needle complex. Activation of the T3SS impairs the secretion of the early substrates but triggers the secretion of the Yop effectors (late substrates) (10, 11). This modification of the secretion pattern was first described by Macnab and co-workers (12–14) in the flagellum and is called the substrate specificity switch. It has been shown that YscP plays a critical role in regulating the needle length (15–18). An YscP-null mutant or insertions within the YscP sequence triggered the formation of long needles. in contrast, shorter needles were produced when deletions were introduced in the YscP sequence (19). Furthermore, a minimal needle length is required to support Yop secretion (17). Together, these results suggest that the needle length is tightly regulated and that YscP functions as a molecular ruler (16). Although the ruler model has attracted significant interest, alternative models of needle length control such as the measuring cup model (15) and the molecular clock model (20) have also been proposed, and there is currently no consensus regarding the true nature of the needle length control mechanism. A systematic deletion analysis of YscP in *Yersinia enterocolitica* led to the identification of domains with specific functions (11, 19), including two distinct

* This work was supported by Swedish Research Council Grants 2013-5954 (to M. W.-W.) and 2015-02874 (to H. W.-W). The authors declare that they have no conflicts of interest with the contents of this article.
[S] This article contains supplemental Figs. 1–9 and Tables S1 and S2.
[1] To whom correspondence may be addressed: Dept. of Clinical Medicine, Bartholins Allé 6, Bldg. 1245, Aarhus University, 8000 Aarhus C, Denmark. E-mail: frederic.login@clin.au.dk.
[2] To whom correspondence may be addressed: Dept. of Chemistry, Bldg. KBC, A3 Linnaeus väg 10, Umeå University, 90187 Umeå, Sweden. E-mail: magnus.wolf-watz@umu.se.
[3] The abbreviations used are: T3SS, type III secretion system; Yop, *Yersinia* outer protein; HSQC, heteronuclear single quantum coherence; ITC, isothermal titration calorimetry; K_d, dissociation constant; Tricine, *N*-[2-hydroxy-1,1-bis(hydroxymethyl)ethyl]glycine; TCEP, tris(2-carboxyethyl)-phosphine; IPTG, isopropyl β-D-1-thiogalactopyranoside; MBP, maltose-binding protein.

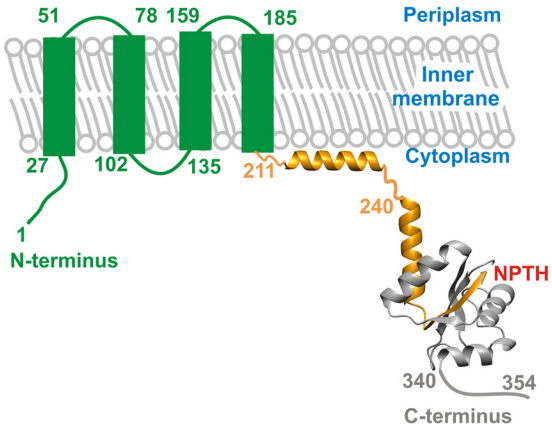

FIGURE 1. **Schematic representation of the YscU domain architecture.** YscU features an N-terminal inner membrane-interacting domain (*green*) consisting of four transmembrane α helices, which were predicted using the TMHMM server. The cytoplasmic domain of YscU, denoted $YscU_C$, has been crystallized with a construct comprising residues 240–339 (Protein Data Bank code 2JLI) and is shown in a schematic representation (25). The NPTH motif is indicated in *red*, and the polypeptides resulting from autocleavage are colored *orange* ($YscU_{CN}$) and *gray* ($YscU_{CC}$), respectively. The linker sequence (residues 211–239) connecting the N-terminal domain with $YscU_C$ has been shown to interact with the inner membrane (25–27) and is modeled as an α helix.

secretion signals (residues 1–35 and residues 97–137) and a substrate specificity switch domain located between residues 385 and 500 (11). Homologues of YscP with similar functions are found in the flagella and T3SSs of diverse bacterial species (21, 22).

YscU in *Yersinia* spp. and FlhB in the flagellum have also been linked to the substrate specificity switch (23). YscU is anchored in the inner membrane via four transmembrane helices and possesses a large C-terminal cytoplasmic domain named $YscU_C$ (Fig. 1) (24, 25). $YscU_C$ is characterized by a conserved NPTH motif that undergoes an autoproteolytic process (between Asp^{263} and Pro^{264}) to generate a C-terminal peptide named $YscU_{CC}$ that form a stable complex with the N-terminal part of the cytoplasmic domain named $YscU_{CN}$. Previous results obtained in our laboratories suggest that the positively charged residues within the linker between $YscU_C$ and the membrane domain interact with the membrane lipids to associate $YscU_C$ with the inner membrane (26). Accordingly, it has been shown that mutations at Asp^{263} or Pro^{264} that block YscU autoproteolysis interfere with both needle formation and Yop secretion (10, 27). Also, we have shown that the dissociation of $YscU_C$ is required for Yop effector secretion (28). It was subsequently found that $YscU_C$ contains a C-terminal secretion signal domain (29). The deletion of the last 15 residues of YscU triggered an increase in YscF secretion without affecting Yop secretion (29). Thus, like YscP, YscU is involved in the substrate specificity switch. Similar results were reported for FliK and FlhB, which are the flagellar homologues of YscP and YscU, respectively (30, 31). Interestingly, the phenotype observed in a *yscP*-null mutant was partially suppressed by single amino acid substitutions within YscU ($YscU^{A268F}$, $YscU^{Y287G}$, and $YscU^{V292T}$) (10). It was subsequently shown that these suppressor mutants are less stable and exhibit faster dissociation kinetics than the wild-type protein, which enabled Yop secretion to occur in the absence of YscP (10, 28). Direct interactions have been observed between FlhB and FliK (*Salmonella enterica* serovar Typhimurium) and between the homologous proteins in *Pseudomonas aeruginosa*, PscU and PscP (residues 31–36), supporting the proposed functional link between YscU and YscP homologues (10, 21, 22).

The homologue of YscI in *S. enterica* serovar Typhimurium, PrgJ, has been proposed to form the inner rod, a structure that connects the needle to the basal body (20, 32). A study on *Yersinia pseudotuberculosis* showed that both YscP and YscU regulate YscI export (33). Indeed, YscI secretion by the T3SS is increased in a *yscP*-null mutant, whereas mutations in $YscU_C$ reduced the secretion level of YscI in a Δ*yscP* strain. Interestingly, it was also recently shown that in *Y. enterocolitica* YscI is required for the export of YscP-PhoA hybrid into the periplasm (34). Moreover, an interaction between EscI and EscU (homologues of YscI and YscU, respectively) in *Escherichia coli* has been reported (35).

Here we report data regarding the interactions among YscU and the two proteins YscP and YscI. Using NMR spectroscopy, we showed that YscP binds to the C-terminal helix of YscU. The A335N point mutation within the YscP binding interface of $YscU_C$ disrupted YscU-YscP interaction without affecting the $YscU_C$ structure. The interaction was found to be functionally significant, and a *yscU*-null mutant expressing the $YscU^{A335N}$ variant did not secrete Yops into the culture supernatant and did not induce cytotoxicity in HeLa cells. Furthermore, unlike a Δ*yscP* mutant or YscU mutants in the NPTH motif, $YscU^{A335N}$ did not promote secretion of the needle subunit YscF. These results suggest that the YscU-YscP interaction is critical for secretion of both early and late substrates. In addition, we found that binding of YscP to the slowly autocleaving mutant $YscU_C^{P264A}$ reduced the rate constant of the autocleavage event *in vitro*. This finding suggests that the binding of YscP to $YscU_C$ can regulate the autocatalytic event, which in turn would affect the ability of $YscU_C$ to dissociate and the subsequent secretion of its C-terminal polypeptide ($YscU_{CC}$). Finally, data from isothermal titration calorimetry and pulldown assays show that YscI interacts with $YscU_C$ but not with either of the polypeptides resulting from autoproteolysis and dissociation ($YscU_{CN}$ and $YscU_{CC}$).

Results

YscU Binds to the Disordered Segment of YscP—Previous genetic analysis showed that *yscP* deletion abolishes Yop secretion and that the wild-type phenotype can be partially rescued by the A268F, Y287G, and V292T suppressor mutations within YscU (10). Based on these results, it was proposed that an interaction between YscP and YscU was critical for Yop secretion. Here we characterize the interaction between the cytoplasmic domain of YscU ($YscU_C$) and YscP using NMR spectroscopy. A direct interaction between YscP and $YscU_C$ homologues in *P. aeruginosa* (denoted PscP and $PscU_C$, respectively) has been observed previously by NMR (22); it was shown that a conserved N-terminal segment of PscP was responsible for its interaction with $PscU_C$. The domain architecture of PscP has been described as a "ball-and-chain" topology where the "ball", *i.e.* the C-terminal domain, is folded and believed to function as a substrate switch, whereas the N-terminal "chain" polypeptide

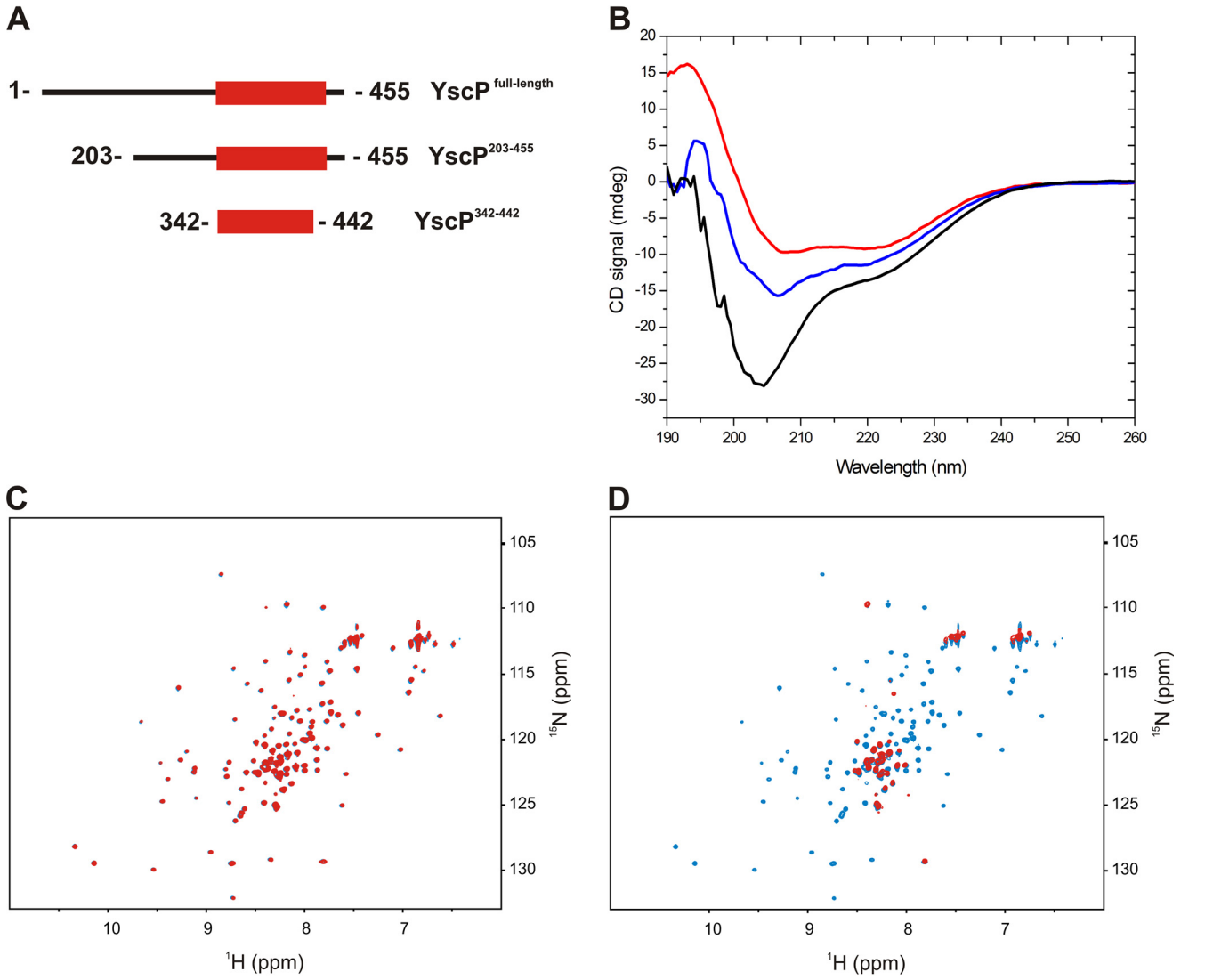

FIGURE 2. **YscP domain architecture and its $YscU_C$-interacting segment.** *A*, schematic representation of YscP and its truncated variants that were used in this study. *B*, far UV-CD spectra of YscP (*black*), YscP(342–442) (*red*), and YscP(203–455) (*blue*). All proteins were used at a concentration of 10 μM in 5 mM sodium phosphate, 30 mM NaCl, 1 mM DTT (pH 7.4) at 20 °C. *mdeg*, millidegrees. *C*, overlay of two-dimensional ^{1}H-^{15}N HSQC spectra of free ^{15}N-labeled $YscU_C$ (*blue*) and ^{15}N-labeled $YscU_C$ mixed with unlabeled YscP(342–442) (*red*). *D*, overlay of two-dimensional ^{1}H-^{15}N HSQC spectra of free ^{15}N-labeled $YscU_C$ alone (*blue*) and mixed with unlabeled YscP(203–455) (*red*).

is disordered and flexible in solution (22). A similar architecture has been determined for the YscP homologue FliK from *S. enterica* serovar Typhimurium (21). A multiple sequence and structural alignment of YscP with FliK, PscP, and other homologues (supplemental Fig. 1) suggests that YscP has a structural topology resembling those described for FliK and PscP.

To investigate the domain architecture of YscP, we used three constructs (Fig. 2*A*) that were designed based on the results of a limited proteolysis experiment of YscP (supplemental Fig. 2) and a multiple sequence alignment (supplemental Fig. 1). These YscP variants were subjected to structural analysis using NMR and circular dichroism (CD) spectroscopy. First, size exclusion chromatography was used to determine the oligomeric state of YscP, YscP(342–442), and YscP(203–455) in solution. Interestingly, although the full-length YscP migrated as a 50-kDa monomer, YscP(342–442) and YscP(203–455) eluted with the column void volume, suggesting that both truncated variants aggregated in solution (supplemental Fig. 3). A CD spectrum of full-length YscP (Fig. 2*B*) indicated that the protein contained both unstructured and structured regions, and this was confirmed by the observation of bands at 205 and 220 nm in their CD spectra. The structured region of YscP was assigned to the C terminus of the protein by analyzing the CD spectra of the two truncated variants (YscP(203–455) and YscP(342–442)). To confirm that YscP(342–442) contained a structured domain, we acquired a ^{1}H-^{15}N HSQC spectrum of a sample of the protein that was isotopically enriched with $^{15}NH_4Cl$. This NMR spectrum conclusively demonstrated that YscP(342–442) is a folded domain because it exhibits the large chemical shift dispersion typical of well folded proteins (supplemental Fig. 4). Although folded, the domain displayed tendencies to aggregate. The NMR spectrum was acquired at a concentration of 50 μM, and any increase in concentration resulted in precipitation of the protein. These results together demonstrate that YscP has a ball-and-chain domain architecture like its homologues. Next, we investigated the interaction

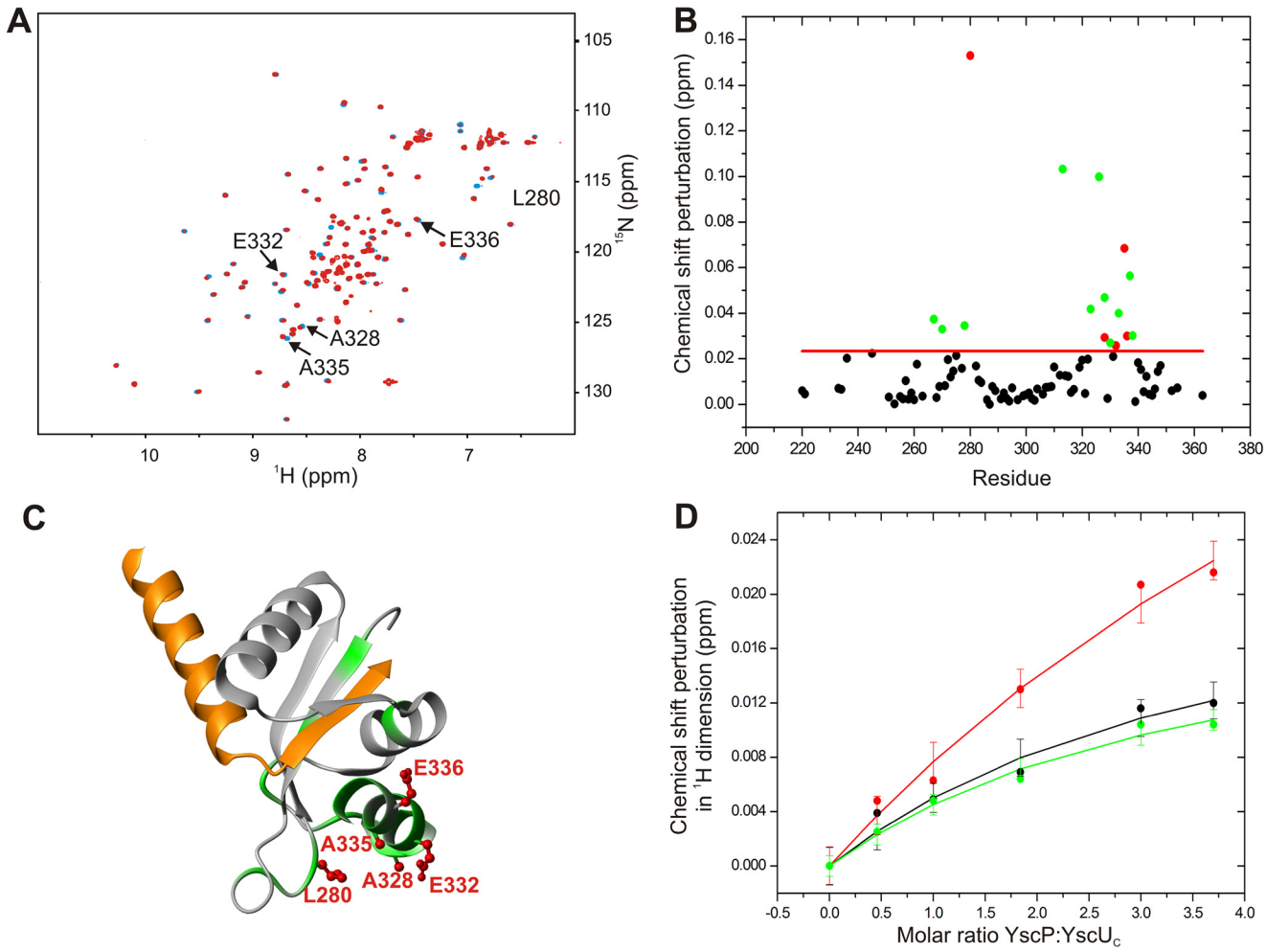

FIGURE 3. **NMR-based identification of the YscP binding surface on YscU$_C$.** *A*, overlay of the two-dimensional ^{1}H-^{15}N HSQC spectra of free ^{15}N-enriched YscU$_C$ (100 μM) before (*blue*) and after addition of YscP (400 μM) (*red*). The spectra were acquired in PBS buffer containing 1 mM TCEP at 37 °C. Solvent-exposed residues that exhibit significant chemical shift perturbations upon YscP addition are marked with *arrows*. *B*, compounded chemical shift perturbations (ppm) between free ^{15}N-labeled YscU$_C$ and ^{15}N-labeled YscU$_C$ in complex with unlabeled YscP were calculated using Equation 1 and plotted against the YscU$_C$ primary sequence. The threshold value used to define a significant chemical shift perturbation is indicated by the *red line*, and residues exhibiting significant shifts are represented by *green dots* except for solvent-accessible amino acid residues with significant chemical shift perturbations (Leu^{280}, Ala^{328}, Glu^{332}, Ala^{335}, and Glu^{336}), which are represented by *red dots*. *C*, display of the YscP binding interface on YscU$_C$. The structure of YscU$_C$ illustrates the positions of the residues with significant chemical shifts (*green*) and the solvent-exposed residues with significant chemical shift perturbations (indicated as *red ball and sticks*). *D*, determination of the K_d value for the YscP-YscU$_C$ interaction obtained by using Equation 2 to fit the changes in the chemical shifts of the methyl groups of YscU$_C$ induced by YscP addition. Plots for three peaks in the methyl region are shown in *black*, *red*, and *green*, respectively. The *error bars* represent S.D.

between YscP and YscU$_C$ by observing perturbations in the ^{1}H-^{15}N HSQC spectrum of ^{15}N-isotopically enriched YscU$_C$ upon addition of the different YscP constructs. In general, interactions between partners in such cases induce changes in the chemical shifts or the line width of the peaks in the spectrum depending on the molecular masses of the interacting partners. The addition of YscP(342–442) did not trigger any changes in the NMR spectrum of YscU$_C$ (Fig. 2*C*), suggesting that this YscP segment does not harbor the YscU$_C$ interaction interface. In contrast, we observed extensive line broadening of the YscU$_C$ resonances when YscP(203–455) was added (Fig. 2*D*), indicating that YscU$_C$ becomes integrated into a high molecular weight complex following the addition of YscP(203–455). Based on this analysis, we propose that the YscU$_C$ binding segment on YscP is localized between residues Glu^{203} and Arg^{341}.

YscP Interaction Interface on YscU$_C$—Despite intensive studies on YscP and YscU homologues, there are no high resolution structural data on the interaction interface on YscU$_C$ responsible for its interaction with YscP. We identified this interaction interface using NMR spectroscopy by titrating unlabeled YscP to ^{15}N-labeled YscU$_C$. The stepwise addition of unlabeled YscP to ^{15}N-labeled YscU$_C$ caused localized perturbations in the chemical shifts of the amide proton and nitrogen resonances of several YscU$_C$ residues in the ^{1}H-^{15}N HSQC spectrum of the protein (Fig. 3*A*). The binding interface was identified by displaying the residues with significant compounded chemical shift perturbations on the YscU$_C$ structure (Fig. 3*B*). As expected for a well defined interaction interface, the YscP-interacting residues on YscU$_C$ cluster to form a contiguous surface; the solvent-exposed residues Leu^{280}, Ala^{328}, Glu^{332}, Ala^{335}, and Glu^{336} seem to form the YscP interaction interface. Interestingly, the interaction interface is centered on the C-terminal α helix of the YscU C-terminal domain (YscU$_{CC}$) (Fig. 3*C*). The titration experiment also enabled us to estimate the binding affinity (dissociation constant (K_d)) of the YscP-YscU$_C$

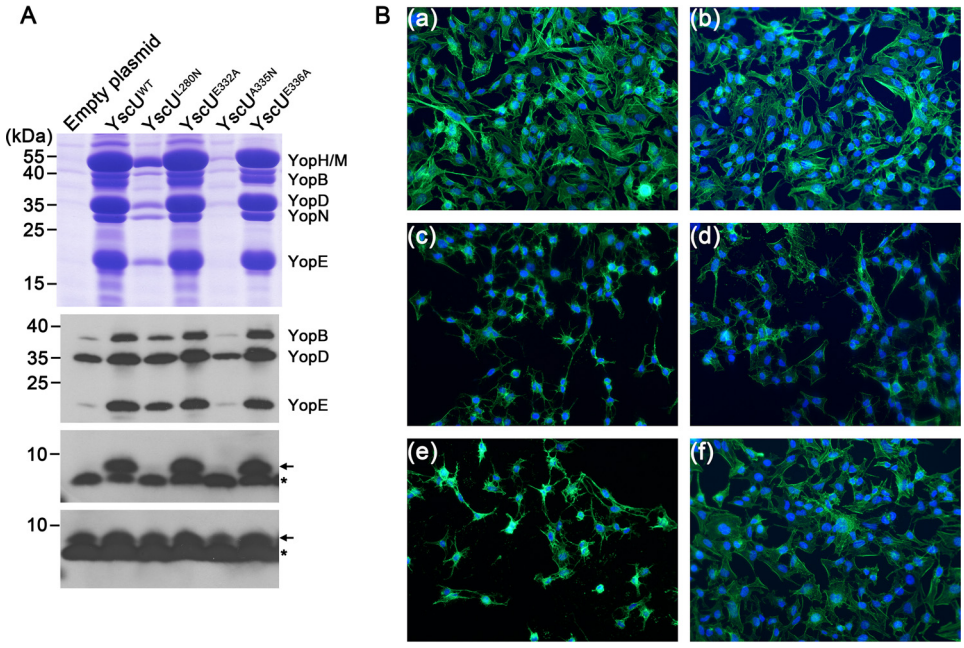

FIGURE 4. **Secretion profiles and cytotoxicity of *Y. pseudotuberculosis* expressing various point mutants of YscU.** *A*, secretion profiles of *Y. pseudotuberculosis* strain YPIII/pIB75 transformed with plasmids encoding different point mutants of YscU. Culture supernatants were precipitated with TCA, separated on a Tris/Tricine gel, and stained with Coomassie R-250 (*upper panels*). Cell pellets of the corresponding strains were analyzed with anti-Yop antibody (*second panel from the top*). The amounts of secreted YscF (*third panel from the top*) and intracellular YscF (*bottom panel*) were analyzed using an anti-YscF antibody. The position of YscF is indicated by the *black arrows*, and the *black asterisks* indicate an unspecific band. *B*, HeLa cells were infected with bacteria at a multiplicity of infection of 10 for 45 min. After fixation with formaldehyde, the cytoskeleton actin filaments were stained with *green* phalloidin-Alexa Fluor 488 (Invitrogen) and nucleic acids were stained with DAPI (*blue*). Uninfected HeLa cells (*panel a*) exhibited non-cytotoxic morphologies similar to cells infected with strains bearing the empty plasmid (*panel b*). Cytotoxicity was observed for 100% of HeLa cells infected with the strains expressing $YscU^{WT}$ (*panel c*) and $YscU^{E332A}$ (*panel e*). $YscU^{L280N}$ induced delayed cytotoxicity (*panel d*). $YscU^{A335N}$ generated no cytotoxicity (*panel f*).

interaction by monitoring changes in the chemical shifts of the methyl resonances of $YscU_C$ as the concentration of YscP increased (Fig. 3*D*). These data were then fitted to an analytical function based on an assumed two-state binding reaction. The best fitted binding isotherm gave a K_d value of 430 ± 293 μM. Although the estimated K_d value suggests that the YscU-YscP interaction is relatively weak under our experimental conditions, this interaction may be modulated *in vivo* by other factors such as membrane anchoring (26) and/or additional protein partners.

Mutations at the YscU/YscP Binding Interface Regulate Yop and YscF Secretion—Based on the results presented above, we hypothesized that the interaction of YscU with YscP is mediated by the residues Leu^{280}, Ala^{328}, Glu^{332}, Ala^{335}, and Glu^{336}. To test our hypothesis and determine the physiological relevance of the YscU-YscP interaction, we performed a scanning mutagenesis analysis targeting these residues. The point mutations L280N, A328N, E332A, A335N, and E336A were separately introduced into the *yscU* coding sequence and cloned into the pBADmycHis-A plasmid. The resulting plasmids were then transformed into the pIB75 (Δ*yscU*) strain, which carries an in-frame deletion of the *yscU* gene. The ability of the different YscU variants to complement Yop secretion was assayed by culturing the cells in Ca^{2+}-depleted medium with a temperature shift from 26 to 37 °C. These growing conditions mimic the host cell contact required for activation of secretion via the T3SS and lead to a massive secretion of Yop into the culture supernatant. The empty plasmid and the plasmid encoding $YscU^{WT}$ were used as negative and positive controls, respectively. As expected, Yop secretion was restored by the plasmid encoding $YscU^{WT}$, and no Yop was detected in the supernatant of the strain carrying the empty plasmid (Fig. 4*A*). Similar amounts of Yop were detected in the supernatants of the strains expressing $YscU^{WT}$, $YscU^{E332A}$, and $YscU^{E336A}$ (Fig. 4*A*). Thus, mutating residue Glu^{332} or Glu^{336} to alanine did not affect the function of YscU or the secretion of Yop via the T3SS. Given that the YscU-YscP interaction is required for Yop secretion, this result suggests that Glu^{332} and Glu^{336} may not be important residues for the binding of YscP to YscU. On the other hand, the mutation A335N drastically reduced the secretion of Yop into the supernatant (Fig. 4*A*, *upper panel*). The strain expressing $YscU^{L280N}$ exhibited an intermediate phenotype with a decrease of about 80% of the Yop secreted by the wild type (Fig. 4*A*, *upper panel*). Lower amounts of intracellular Yop were detected for the strains bearing the empty plasmid or the plasmid expressing $YscU^{A335N}$ (Fig. 4*A*). The attenuation of Yop secretion represses the expression of the *yop* genes, reducing the intracellular amount of the corresponding proteins. The ability of these different variants to generate a cytotoxic phenotype in HeLa cells was also assayed. Unlike $YscU^{WT}$ and $YscU^{E332A}$, no cytotoxicity was generated by $YscU^{A335N}$ (Fig. 4*B*), and the appearance of the cytotoxicity phenotype was delayed for $YscU^{L280N}$ (Fig. 4*B*). Thus, both Yop secretion and translocation are affected by the A335N and L280N mutations. Taken together, these results indicate that Ala^{335} and Leu^{280} are critical for the interaction of YscU with YscP and Yop secretion via the T3SS. These mutations also impaired the secretion of the needle subunit YscF (Fig. 4*A*, *third and fourth panels from*

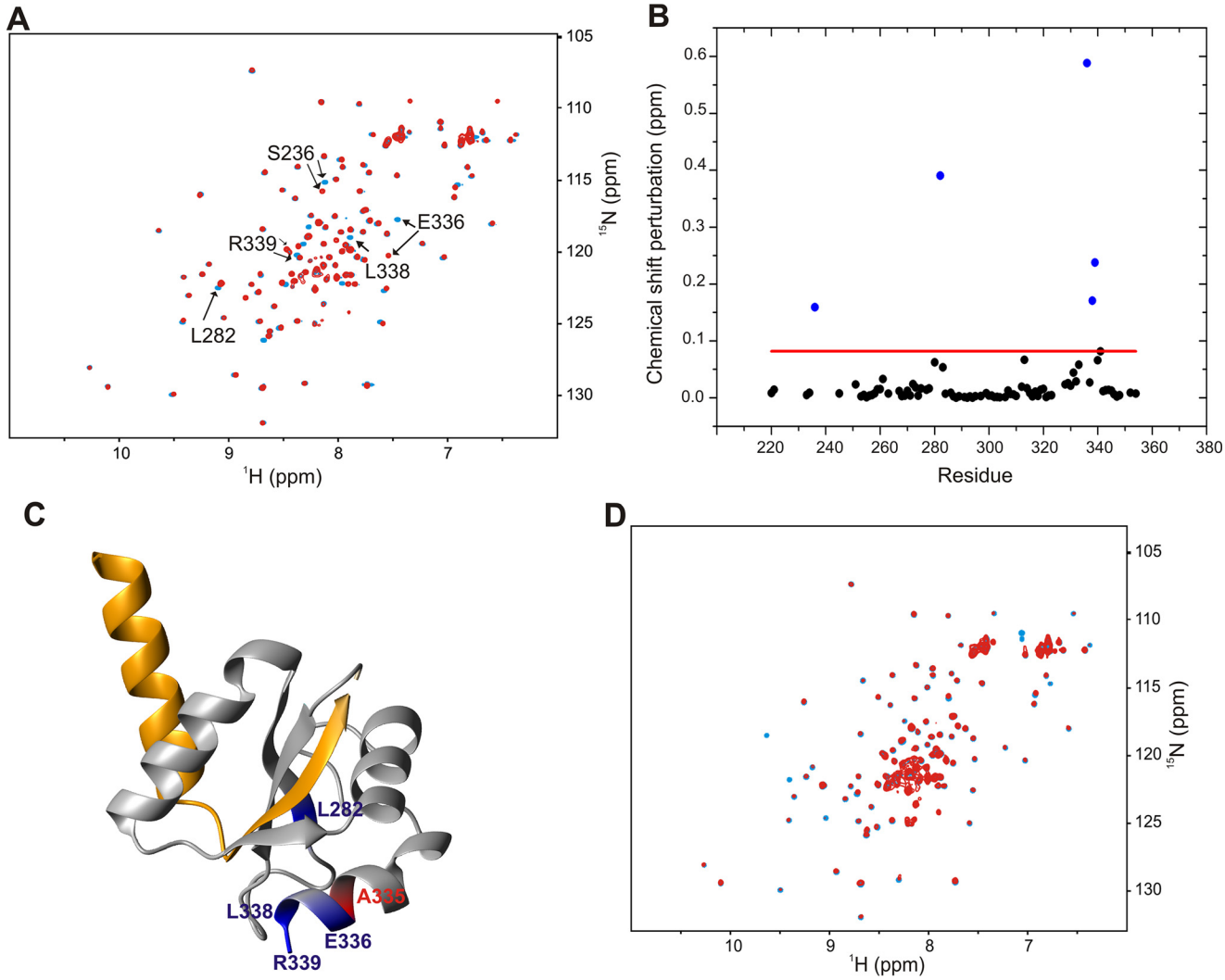

FIGURE 5. **Disruption of YscP binding by the A335N replacement in YscU$_C$.** *A*, overlay of two-dimensional ^{1}H-^{15}N HSQC spectra of ^{15}N-labeled YscU$_C^{WT}$ (*blue*) and YscU$_C^{A335N}$ (*red*) at concentrations of 100 μM. The buffer consisted of PBS and 1 mM TCEP at 37 °C. Solvent-exposed residues that exhibit significant chemical shift perturbations upon mutation are indicated with *arrows*. *B*, compounded chemical shift perturbations (ppm) between ^{15}N-labeled YscU$_C^{WT}$ and ^{15}N-labeled YscU$_C^{A335N}$ calculated by Equation 1 and plotted against the YscU residue number. The threshold value used to define significant chemical shift changes is indicated by the *red line*. The residues with the largest chemical shift perturbations (Ser^{236}, Leu^{282}, Glu^{336}, Leu^{338}, and Arg^{339}) cluster around the mutation site and are shown in *blue*; position 335 is shown in *red* on the YscU$_C$ crystal structure in *C*. *D*, overlay of two-dimensional ^{1}H-^{15}N HSQC spectra of ^{15}N-labeled YscU$_C^{A335N}$ at a concentration of 100 μM alone before (*blue*) and after addition of unlabeled YscP (*red*) at a molar ratio of 1:4 in PBS.

the top). YscF is an early substrate, whereas Yop is a late substrate (34). Previous studies showed that the substrate specificity switch from early to late substrates is regulated by both YscU and YscP (10). The absence of YscF in the supernatant of the strain expressing YscU^{A335N} suggests that this mutation affects the secretion of both early and late substrates.

The results of the complementation analysis presented above showed that the residue Ala^{335} is critical for the function of YscU. The A335N mutation could thus impair either the folding of YscU or its interaction with YscP. To determine whether the A335N mutation affects the structure of YscU, we acquired a ^{1}H-^{15}N HSQC spectrum of YscU$_C^{A335N}$ and compared it with that of the wild type. An overlay of the two spectra revealed no significant differences in chemical shifts, and the majority of their cross-peaks have similar intensities and positions (Fig. 5*A*). The only residues that showed significant chemical shift perturbations are in close proximity to the mutation site, so we can conclude that the mutation does not affect the overall structure of YscU$_C$ (Fig. 5, *B* and *C*). We then investigated whether YscU$_C^{A335N}$ retained the ability to interact with YscP by performing an NMR titration of unlabeled YscP against ^{15}N-labeled YscU$_C^{A335N}$ at 37 °C (Fig. 5*D*) as we had done previously with YscU$_C^{WT}$. A comparison of the spectra from the titrations of YscP against YscU$_C^{WT}$ and YscU$_C^{A335N}$ showed that the chemical shift perturbations of YscU$_C^{A335N}$ were significantly smaller than for YscU$_C^{WT}$ (Fig. 5*D*). Furthermore, a K_d value for the interaction between YscU$_C^{A335N}$ and YscP could not be quantified because the chemical shift changes were too small (supplemental Fig. 5). These data clearly indicate that the YscU$_C^{A335N}$ mutant retains the structure of the wild-type protein but has lost its YscP binding activity.

YscP Protects the Slow Processing Mutant P264A from Autocleavage—It has been shown previously that the dissociation of YscU$_C$ into the two polypeptides YscU$_{CC}$ and YscU$_{CN}$ is required for Yop secretion and that YscU$_{CC}$ is subsequently secreted into the culture supernatant (27, 29). The secretion of

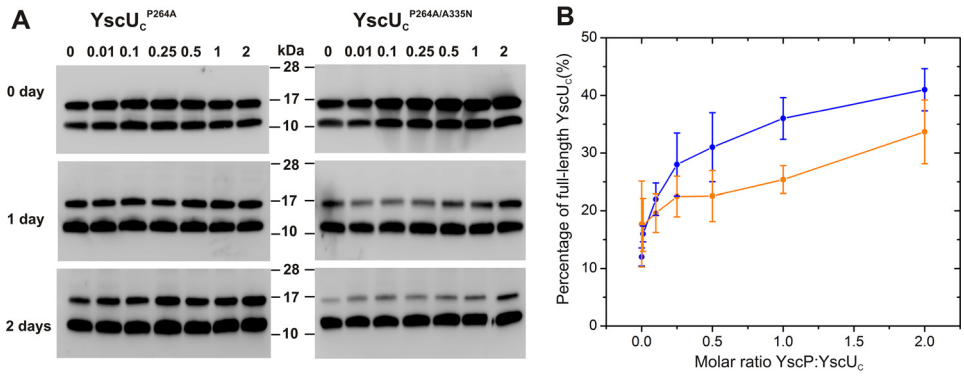

FIGURE 6. **YscP binding attenuates the rate of YscU autocleavage.** *A*, immunoblotting detection of the degree of autocleavage of YscUC^{P264A} and YscU$_C^{P264A/A335N}$ using anti-YscU$_{CC}$ as the primary antibody. Autocleavage was monitored over 2 days at 37 °C with varying concentrations of YscP. The YscU$_C$:YscP ratio was varied from 0 to 2 as indicated at the *top* of the figure. Each sample shows two bands in the immunoblot: the *top band* corresponds to uncleaved YscU$_C$, whereas the *lower band* corresponds to the YscU$_{CC}$ polypeptide. *B*, the immunoblotting experiments were analyzed by quantifying the proportion of uncleaved YscU$_C^{P264A}$ (*blue*) and YscU$_C^{P264A/A335N}$ (*orange*) in the samples after 2-day incubation. Values shown in the graph are means with *error bars* representing ± S.D. (the experiment was repeated four times).

YscU$_{CC}$ through the T3SS is facilitated by a C-terminal secretion sequence, and the non-secreting phenotype observed for *yscP*-null mutants is partially rescued by the secondary suppressor mutants YscU^{A268F}, YscU^{Y287G}, and YscU^{V292T} (10, 33). These suppressor mutants display elevated rate constants for the dissociation of YscU$_C$ into YscU$_{CN}$ and YscU$_{CC}$ relative to wild-type YscU$_C$ (28). To determine whether YscP can affect the dissociation of YscU$_C$, we studied the dissociation kinetics of YscU$_C$ in the absence and presence of YscP by NMR spectroscopy as described previously (28). The experiments revealed that YscP does not significantly change the dissociation kinetics of YscU$_C$ (supplemental Fig. 6). It is important to note that wild-type YscU$_C$ is fully cleaved in these experiments because of the protein's long handling time during purification. To determine whether YscP can modulate the rate of autoproteolysis, we studied the slowly autocleaving mutant P264A (27) whose autoproteolysis proceeds slowly enough to allow purification of partially uncleaved protein. The *in vitro* cleavage kinetics of this mutant into the two polypeptide fragments YscU$_{CN}$ and YscU$_{CC}$ can be followed by Western blotting with an anti-YscU$_{CC}$ antibody (Fig. 6 and supplemental Fig. 7) at 37 °C at 0, 1, and 2 days after purification. Each sample generated two bands in the immunoblot due to the incomplete autoproteolysis of the YscU$_C^{P264A}$ variant; the uppermost band corresponded to uncleaved YscU$_C$, and the lower band corresponded to the cleaved YscU$_{CC}$ polypeptide (Fig. 6). The total protein content for each sample was calculated from the sum of the bands corresponding to YscU$_C$ and YscU$_{CC}$. The relative abundance of the uncleaved full-length protein (*i.e.* YscU$_C$ variant) was then calculated as the percentage of total protein concentration. Following this analysis, it is evident that YscP can reduce the rate of YscU$_C^{P264A}$ autoproteolysis in a concentration-dependent manner (Fig. 6). To test whether the effect is specific, we turned to the double mutant YscU$_C^{P264A/A335N}$, which has both slow autoproteolysis and a weakened YscP binding affinity. The YscP dose dependence for the protection against autoproteolysis is significantly weaker for the double mutant in comparison with the YscU$_C^{P264A}$ single mutant. This observation suggests that the effect on autoproteolysis mediated by YscP is specific and driven by the interaction of YscP with the identified binding surface of YscU$_C$. Taken together, the data show that YscP can protect the slowly cleaving YscU$_C$ mutant P264A from autoproteolysis *in vitro*.

YscU Binds to the Inner Rod Protein YscI at Molar Ratio 1:1—The proposed T3SS structural model suggests that the protein YscI (*Yersinia* spp.), MxiI (*Shigella* spp.), or PrgJ (*Salmonella* spp.) polymerizes into an inner rod to form a conduit for protein secretion through the periplasm (20, 33, 36, 37). YscI is secreted via the T3SS, and it has been shown that YscI secretion is regulated by both YscP and YscU (33). It has also been shown that the inner rod protein EscI, a homologue of YscI in enteropathogenic *E. coli* interacts with the YscU homologue EscU (35). We therefore investigated whether YscU interacts with YscI and attempted to determine the binding interface (Fig. 7) by performing GST pulldown experiments in which YscU$_C$, YscU$_{CN}$, and YscU$_{CC}$ were GST-tagged and used as bait to co-purify YscI-His$_6$. YscI-His$_6$ only bound to GST-YscU$_C$; no YscI remained associated to GST alone, GST-YscU$_{CN}$, or GST-YscU$_{CC}$ (Fig. 7*A*). This interaction pattern suggests that the interaction of YscI with YscU$_C$ is abolished by the dissociation of YscU$_{CC}$ from YscU$_{CN}$ and/or structural changes of YscU$_{CC}$ and YscU$_{CN}$. To further characterize the binding of YscI to YscU, we analyzed this interaction using isothermal titration calorimetry (ITC) (Fig. 7*B*). The binding is characterized by a distinct exothermic binding process that can be robustly fitted to a one-site binding model (Fig. 7*B*) with a K_d of 3.8 μM and a 1:1 stoichiometry.

Previous structural analyses of two YscI homologues, MxiI and PrgJ, using CD and NMR spectroscopy have shown that they are partially folded in solution (36). Although MxiI, PrgJ, and YscI have equivalent functions in the T3SS, their sequence similarity is relatively low (supplemental Fig. 8). The CD spectrum of YscI features distinct CD bands in the region between 205 and 220 nm, which is indicative of significant secondary structure content (Fig. 7*C*).

We attempted to characterize the binding interface of YscI on YscU$_C$ by performing two-dimensional NMR experiments. A titration of unlabeled YscI against ^{15}N-labeled YscU$_C$ resulted in massive line broadening of the peaks corresponding to YscU$_C$ residues due to aggregation of YscI in solution into

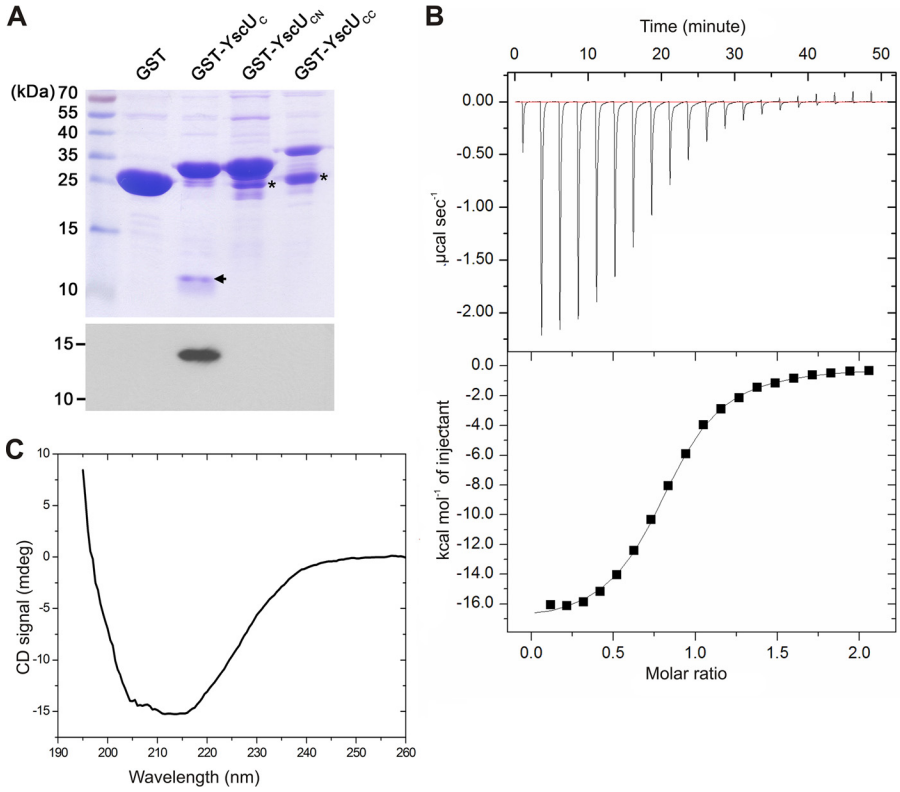

FIGURE 7. **The inner rod protein YscI interacts with YscU$_C$ but not with YscU$_{CN}$ or YscU$_{CC}$.** *A*, GST pulldown assay using different variants of YscU and polyhistidine-tagged YscI. *Top panel*, verification of binding of GST, GST-YscU$_C$, GST-YscU$_{CN}$, and GST-YscU$_{CC}$ to glutathione-Sepharose beads. This was accomplished by applying aliquots of the different proteins to glutathione-Sepharose beads, extensive washing to remove unbound material, and subsequent SDS-PAGE analysis of aliquots of beads bearing the bound proteins. The gels were stained with Coomassie R-250 for detection. *Black asterisks* indicate degradation products. *Bottom panel*, GST and GST-tagged YscU variants were incubated with purified YscI. After several washes, resin-associated proteins were eluted and separated on the gel for immunoblotting detection with an anti-His$_6$ antibody. The *black arrow* indicates the position of YscU$_{CC}$ in the GST-YscU$_C$ sample. *B*, raw data from an ITC experiment involving addition of YscU$_C$ to YscI are shown in the *upper panel*; the *lower panel* shows the integrated heats obtained after subtracting the heat of dilution. The best fitting binding isotherm is shown as a *solid line*. The fitted parameters are $K_d = 3.8$ µM, $\Delta H^0 = -17$ kcal mol^{-1}, $\Delta S^0 = -33.8$ cal mol^{-1} degrees^{-1}, and a stoichiometry "*n*" of 0.8 at 25 °C. *C*, far-UV CD spectrum of YscI. The experiment was conducted with 10 µM YscI in a 5 mM sodium phosphate buffer (pH 7.4) containing 30 mM NaCl and 1 mM DTT at 25 °C. *mdeg*, millidegrees.

complexes that are too large to permit the detection of YscI-bound YscU$_C$ resonances. However, a two-dimensional ^{1}H-^{15}N HSQC experiment using ^{15}N-labeled YscU$_C^{A335N}$ showed that the binding of YscI was not abolished by the mutation A335N in contrast to that of YscP (supplemental Fig. 9). The interactions of YscP and YscI with YscU thus appear to occur at different binding surfaces.

Discussion

Type III secretion systems are complex nanomachines spanning the cell wall of Gram-negative bacteria. They are constituted by around 25 proteins whose assembly requires that the individual components are added in a specific order (38). Furthermore, the T3SS substrates (Yops in *Yersinia*) that are destined for the eukaryotic cytosol are not exported before cell contact between the pathogen and the eukaryotic target cell has been established (39). Thus, there exists a secretion hierarchy allowing early T3SS substrates to be secreted before the secretion of the late substrates is allowed. This process was first described for the flagellar T3SS and was named "substrate specificity switching" by Macnab (12). In *Yersinia* spp., YscP and YscU have been shown to be essential components of the substrate specificity switching mechanism. A *yscP* mutant assembles elongated needles, but it is unable to secrete Yop effectors (19). Similar phenotypes have also been reported for the homologous proteins in *Salmonella* and *Shigella* T3SSs (31, 40). Interestingly mutations in the cytoplasmic domain of *yscU* can suppress a *yscP* mutant phenotype, leading to decreased export of the needle protein YscF and increased Yop secretion (10, 27). These genetic results argue strongly for a direct YscP and YscU interaction that is important to enable *Yersinia* to regulate the substrate switch. YscU and its homologues in other bacteria undergo autocatalytic cleavage at a conserved NPTH motif, generating a C-terminal 10-kDa peptide fragment called YscU$_{CC}$ in *Yersinia*. YscU$_{CC}$ remains bound to the membrane-anchored part of YscU after cleavage (27). Removal of Ca^{2+} from the growth medium results in Yop secretion as well as secretion of YscU$_{CC}$, indicating that YscU is dissociated under these conditions (28). Furthermore, we also showed previously that *yscP* suppressor mutants mapping to the *yscU$_{CC}$* part of the *yscU* gene destabilized the interaction between the two YscU polypeptides generated by autocleavage, indicating that YscU$_{CC}$ dissociation is an essential step in substrate switching in *Yersinia*. It has therefore been proposed in line with these findings that the decisive step in substrate switching is the autocatalytic event and that YscP is a key regulator of this process.

Here we used solution state NMR spectroscopy to identify the YscP binding interaction interface on the cytoplasmic domain of YscU ($YscU_C$). The interaction surface is centered on the C-terminal α helix of $YscU_C$, and disruption of the surface by introducing the A335N point mutation dramatically reduced Yop secretion and cytotoxicity on HeLa cells. On the basis of biophysical analyses with circular dichroism and NMR spectroscopy, we show that YscP has a ball-and-chain architecture with an extended N-terminal flexible segment attached to a folded C-terminal domain. A similar architecture has been demonstrated previously for the orthologue PscP from *P. aeruginosa* (22) and for FliK from *S. enterica* serovar Typhimurium (21). These results suggest that the ball-and-chain architecture is strongly conserved among the YscP class of bacterial proteins. By performing a deletion analysis of YscP, we showed that the protein interacts with YscU via amino acid residues in its disordered N-terminal segment. This is analogous to the scenario observed in *P. aeruginosa* where N-terminal residues of PscP interact with the YscU orthologue PscU (22). It has been proposed that the C-terminal folded domain of PscP is located at the growing tip of the needle structure (22) and that the N-terminal flexible segment spans the entire T3SS to make contact with PscU located in the cytoplasm. This model is consistent with the fact that YscP has been identified as a secreted protein in *Yersinia* (41) and that it is also surface-located. In accordance with these results, YscP has been postulated to function as a "molecular ruler" that defines the correct length of the needle structure (19). An issue that remains to be answered is the nature of the mechanism that enables discrimination between early and late substrates. As discussed, we have shown previously that autoproteolysis of YscU enables secretion of the C-terminal YscU polypeptide ($YscU_{CC}$) and that its secretion parallels that of the Yops (28). Destabilized YscU mutants that displayed increased rate constants of dissociation also enable secretion of Yops at 30 °C, a temperature at which the wild-type strain effectively displays no Yop secretion. In addition, we previously identified a C-terminal secretion signal in $YscU_{CC}$ (29). Taken together, these findings suggest that $YscU_{CC}$ dissociation and subsequent secretion enabled by autoproteolysis play an important role in regulating Yop secretion. However, a contradictory hypothesis exists whereby the role of autoproteolysis is to shape the three-dimensional structure of YscU and thereby enable the protein to engage in downstream protein-protein interactions (42). This hypothesis is supported by the observation that uncleaved SpaS (the YscU orthologue in *Salmonella*) could not be detected inside bacteria. In addition, in an elegant experiment, the authors engineered a SpaS variant that was cleaved by an external protease; also with this experiment no regulatory function of SpaS cleavage could be verified. Taken together, these observations suggest that self-cleavage of SpaS has no regulatory function regarding the substrate specificity switch (42). However, it is possible that the time resolution in the experiments did not allow detection of uncleaved SpaS. Hence, in the context of wild-type SpaS, it is currently problematic to test regulatory aspects of self-cleavage. To test whether autoproteolysis could be regulated in *Yersinia*, we turned to the slowly cleaving $YscU_C$ mutant P264A. The $YscU_C^{P264A}$ mutant has a half-life for autoproteolysis that enables biochemical experiments aimed at probing the role of YscP for the rate of autoproteolysis and/or dissociation. To test for potential effects on $YscU_C$ dissociation kinetics in response to YscP binding, we relied on our established NMR protocol for quantifying this event (28). We could not observe any statistically significant changes in the rate constant of wild-type $YscU_C$ dissociation in the absence or presence of YscP. Using the $YscU_C^{P264A}$ mutant and a protocol based on Western blotting with an antibody against $YscU_{CC}$, we showed that the presence of YscP significantly reduced the rate constant of autoproteolysis. This finding opens the possibility that YscU might be maintained in a state that prevents late substrate secretion when bound to YscP and that release of YscP enables YscU self-cleavage, $YscU_{CC}$ dissociation, and activation of late substrate secretion. This inference is consistent with the model of Bergeron *et al.* (22) where PscP is anchored to PscU on the cytoplasmic side with the N-terminal flexible segment threaded through the needle and the C-terminal folded domain located at the tip of the needle.

It was recently shown by Lloyd and co-workers (33) that the formation of the inner rod by the YscI protein exhibits a critical role in the substrate specificity switch. They also showed that YscU and YscP indirectly control Yop secretion by regulating the export of YscI. These results are in perfect agreement with the view of Marlovits and co-workers (43) who showed that the inner rod was absent in YscP mutants, leading to the conclusion that the inner rod is essential for substrate specificity switching. In addition, it has also been shown that EscI interacts with EscU (35). In line with these observations, we found that YscI interacted with the cytosolic domain ($YscU_C$), but in contrast YscI was unable to interact with either of the two peptides resulting from autoproteolysis. Thus, we conclude that YscI interacts with YscU and that autoproteolysis *per se* does not affect YscI interaction with the two resulting YscU polypeptides as long as they are interconnected. In addition, we recently showed that induction of the switch to late Yop secretion also resulted in secretion of $YscU_{CC}$ (28). This result shows that $YscU_{CC}$ is dislocated from the remaining part of YscU after induction of the switch (28). One possibility based on these findings is that YscU anchors the inner rod to the T3SS and that induction of the switch results in disassociation of the inner rod followed by Yop secretion. In accordance with this hypothesis and the results presented herein, we further suggest that YscP/YscU binding blocks autoproteolysis, and thus $YscU_{CC}$ dissociation followed by YscI release is inhibited. This mechanism requires that $YscU_C$ harbor distinct YscI and YscP binding surfaces, and this feature was established in the current study. In this scenario, YscP could fit very well to serve as the enigmatic T3SS surface sensor because it has also been shown that a domain of YscP is surface-located prior to induction of the switch (41). Thus, YscP can serve as a link between the exterior of the T3SS and proteins regulating the substrate specificity switch, thus fulfilling the basal criteria for a surface sensor. More work is needed in this context, and we now focus our efforts to test this hypothesis.

Experimental Procedures

Bacterial Strains, Plasmids, and Growth Conditions—The bacterial strains and plasmids used in this study are listed in supplemental Table S1. Standard molecular biology methods were used to generate the different plasmid constructs used in the experiments. The PCR primers used in the different clonings are listed in supplemental Table S2. The sequences of all the constructs were verified by sequencing (Eurofins MWG Operon). *E. coli* strains were grown in Luria-Bertani broth (LB) or on Luria agar plates at 37 °C. *Y. pseudotuberculosis* strains were grown at 26 °C in LB or on Luria agar plates. Antibiotics were added to the medium for selection according to the resistance markers carried by the plasmid at the following concentrations: kanamycin, 50 μg/ml; carbenicillin, 100 μg/ml; and chloramphenicol, 35 μg/ml.

Yop Secretion Analysis and Immunoblotting Quantification—To induce Yop secretion, *Y. pseudotuberculosis* strains were first grown at 26 °C for 2 h in Ca^{2+}-depleted LB medium (medium containing 5 mM EGTA and 20 mM $MgCl_2$) and then at 37 °C for 3 h. Cultures were started at an A_{600} of 0.1. Samples were treated as described previously (28) and separated on a Tris-Tricine polyacrylamide gel. Proteins were either stained with Coomassie R-250 or transferred onto a PVDF membrane for immunoblotting. Anti-Yop, anti-His, and anti-YscF antibodies were diluted at 1:5,000. Horseradish peroxidase-conjugated anti-rabbit antibody was diluted at 1:10,000 (GE Healthcare). Proteins were detected with a chemiluminescence detection kit (GE Healthcare).

To monitor the effect of YscP binding on YscU autocleavage, YscP was mixed with 20 μM $YscU_C$ variants at different molar ratios (0, 0.01, 0.1, 0.25, 0.5, 1, and 2) in PBS with 1 mM TCEP and incubated at 37 °C. Samples were taken after 0, 1, and 2 days and diluted to a concentration of 1 μM in the $YscU_C$ variant before mixing with Laemmli buffer (Bio-Rad). The proteins in the samples were then separated by SDS-PAGE and transferred to a PVDF membrane (Bio-Rad) for immunoblotting. Anti-$YscU_{CC}$ was diluted at 1:10,000. Goat anti-rabbit IgG (heavy + light)-HRP conjugate antibody was diluted at 1:20,000. Transferred proteins were detected with a chemiluminescence detection kit (Bio-Rad). Densitometric analysis of the bands was performed using the ImageJ software package based on the same immunoblotting samples (44).

HeLa Cell Cytotoxicity Assay—*Y. pseudotuberculosis* cultures were started at an A_{600} of 0.1 in LB medium containing 1 mM $CaCl_2$. After 1 h of growth at 26 °C, cultures were shifted to 37 °C for 2 h. HeLa cells were infected for 45 min at a multiplicity of infection of 10. Cytotoxicity assays were performed as described by Rosqvist and co-workers (45) with some modifications. For immunostaining, samples were subsequently fixed with 4% paraformaldehyde and permeabilized with 0.5% Triton X-100 (Sigma-Aldrich). Unspecific binding was suppressed by treatment with 0.1 M glycine in PBS containing 1% bovine serum albumin. Alexa Fluor 488-phalloidin (Life Technologies) and DAPI were used to stain the actin cytoskeleton and nucleic acids of the cells, respectively. Samples were mounted in mounting medium (Dako) and examined with a fluorescence microscope (Nikon Eclipse C1 Plus).

Protein Expression and Purification—Proteins produced in the BL21(DE3)/pLysS strain were grown in Luria broth at 37 °C. When an A_{600} of 0.6 was reached, protein production was induced by adding 1 mM isopropyl β-D-1-thiogalactopyranoside (IPTG) to the culture medium and allowing the bacteria to grow for a further 4 h. Bacteria were harvested by centrifugation for 30 min at 5,000 × *g*, and the pellets were frozen at −80 °C. For ^{15}N labeling, bacteria were grown in M9 minimal medium containing $^{15}NH_4Cl$. After addition of 1 mM IPTG at an A_{600} of 0.6, ^{15}N-labeled proteins were isolated from bacteria grown overnight at 30 °C and harvested as described above.

GST-tagged variants of $YscU_C$ and YscP were purified as described previously (28). Bacteria were resuspended in the lysis buffer (50 mM Tris, 100 mM NaCl, 2 mM DTT (pH 7.4)) and lysed by sonication. The lysates were then centrifuged for 30 min at 30,000 × *g* at 4 °C. The supernatant was loaded on a GSTrap column (GE Healthcare) pre-equilibrated with the lysis buffer, the column was washed with 10 column volumes of the same buffer, and then the GST-tagged protein was eluted with 50 mM Tris, 100 mM NaCl, 20 mM glutathione (pH 7.4) buffer. Glutathione was eliminated from the eluate using a centrifugal filter device, and the GST tag was cleaved by incubating the resulting samples with 10 units of PreScission protease (GE Healthcare)/mg of protein overnight at 4 °C. The free GST was eliminated by passing the sample through a GSTrap column with the purified proteins remaining in the column flow-through. The purification of YscP was finalized by loading untagged YscP on a HiPrep 26/60 Sephacryl S-100HR gel filtration column (GE Healthcare) after a buffer exchange to PBS containing 2 mM DTT (pH 7.4). $YscU_C$ was loaded on a Sepharose SP cation exchange column (Sigma-Aldrich) after a buffer exchange to 10 mM Tris containing 25 mM NaCl (pH 7.4) and eluted using an NaCl gradient from 25 to 800 mM in 10 mM Tris (pH 7.4). Both YscP and $YscU_C$ were concentrated in PBS containing 1 mM TCEP (pH 7.4) using centrifugal filter devices.

His_6-YscP(203–455) was produced and lysed as described above. The supernatant was then loaded on a HisTrap column (GE Healthcare). The protein was eluted with an imidazole gradient from 10 to 700 mM in PBS. After removal of imidazole using centrifugal filter units, His_6-YscP(203–445) was loaded on a 26/60 Sephacryl S-100HR gel filtration column.

His_6-maltose-binding protein (MBP)-YscP(342–442) with a double His_6-MBP tag was produced overnight at 25 °C by adding 1 mM IPTG when the A_{600} of the culture reached 0.6. Inclusion bodies were solubilized in 50 mM Tris containing 100 mM NaCl and 8 M urea (pH 7.4). After centrifugation for 30 min at 30,000 × *g* at 4 °C, the supernatant was dialyzed against the same buffer containing 4 M urea for 2 h at 4 °C. The procedure was then repeated with buffers containing 2 M and then 1 M urea. The final dialysis was carried out overnight against 50 mM Tris containing 100 mM NaCl and 10 mM imidazole after which the refolded protein was loaded onto a HisTrap column and eluted with an imidazole gradient from 10 to 700 mM in the loading buffer. The imidazole concentration was then reduced to 10 mM using centrifugal filter devices, and the His_6-MBP tag was removed by overnight incubation at room temperature with 100 units of tobacco etch virus protease/mg of protein. 8 M urea was added to the resulting solution, and the uncleaved

His_6-MBP-YscP(342–442) was removed by affinity chromatography on a HisTrap column with the YscP(342–442) remaining in the flow-through. The buffer was then exchanged to 6 M urea in PBS, and the protein was purified by size exclusion chromatography using a HiPrep 26/60 Sephacryl S-100HR column.

For YscI-His_6 purification, bacteria were resuspended and lysed in 50 mM Tris containing 100 mM NaCl (pH 7.4). The lysates were then centrifuged for 30 min at 30,000 × *g* at 4 °C. Because YscI-His formed inclusion bodies, the pellet was dissolved in a binding buffer of 50 mM Tris containing 100 mM NaCl and 7 M urea (pH 7.4) and then centrifuged. The resulting supernatant was loaded on a HisTrap column, and urea was eliminated by washing the column with a non-urea buffer of 50 mM Tris containing 100 mM NaCl (pH 7.4). The protein was then eluted with an imidazole gradient from 0 to 1 M in 50 mM Tris containing 100 mM NaCl (pH 7.4). Imidazole was eliminated by dialysis overnight at 4 °C into an appropriate buffer for NMR or isothermal titration calorimetry.

NMR Spectroscopy—^{15}N-Labeled proteins were studied at 100 μM in PBS containing 1 mM TCEP and 10% D_2O. In the YscP titration experiments, the quantity of added YscP was chosen to achieve a final concentration of 50, 100, 200, 300, or 400 μM and a $YscU_C$:YscP molar ratio of 0.5, 1, 2, 3, or 4. ^{1}H-^{15}N HSQC spectra were acquired at 37 °C using a Bruker Avance III HD spectrometer at 850 MHz equipped with a 5-mm TCI HCN triple resonance cryoprobe. The NMR spectra were processed with Topspin (Bruker Biospin) or NMRPipe and visualized using ANSIG for Windows (46, 47). Compounded chemical shift perturbations for each backbone ^{1}H-^{15}N signal were computed using the following equation.

$$\Delta\delta\ (\text{ppm}) = |\Delta\delta_H| + 0.2 \times |\Delta\delta_N| \qquad \text{(Eq. 1)}$$

where $\Delta\delta_N$ and $\Delta\delta_H$ are the chemical shift perturbations of the amide nitrogen and amide proton of the assigned residue in the free and complexed forms of the protein, respectively. The calculated chemical shift perturbations were plotted against residue numbers to localize the affected surfaces.

In the binding studies, the chemical shifts of the methyl resonances in ^{1}H one-dimensional NMR spectra of $YscU_C$ were monitored during YscP addition. The YscP-$YscU_C$ interaction occurs under the fast exchange regime on the NMR time scale, so binding constants (K_d) were estimated by fitting the experimental data to Equation 2 based on an assumed 1:1 binding reaction (P + L ↔ PL) where YscP is regarded as "ligand L," $YscU_C$ is regarded as "protein P," and the YscP-$YscU_C$ complex is regarded as "PL". $\Delta\delta_{max}$ is the perturbation of the chemical shift when the binding site is saturated (48).

$$\Delta\delta\ (\text{ppm}) = \frac{\Delta\delta_{\max}}{2}\left(\left(1 + x + \frac{K_d}{P}\right) - \sqrt{\left(1 + x + \frac{K_d}{P}\right)^2 - 4x}\right) \qquad \text{(Eq. 2)}$$

where P is concentration of protein and x is molar ratio of ligand:protein. The reported K_d is an average value based on the individual K_d values of the analyzed peaks.

Limited Trypsin Proteolysis—Limited trypsin proteolysis was utilized to determine the domain architecture of YscP. A 22 μM solution of the full-length YscP protein in PBS was incubated with sequencing grade trypsin (Promega) at ratios of 1:100, 1:1,000, and 1:10,000, and samples were taken after 1-, 5-, 10-, and 20-min incubation at 4 °C. The peptide content of these samples was separated on a 15% SDS-acrylamide gel and stained with Coomassie R-250. The bands corresponding to stable fragments were then excised and identified by ultraperformance liquid chromatography-mass spectroscopy/mass spectroscopy.

CD—Far-UV CD spectra were recorded in a 0.1-cm quartz cuvette on a Jasco J-810 spectropolarimeter equipped with a Peltier element for temperature control. The spectra were recorded using 10 μM protein solutions in 5 mM sodium phosphate, 30 mM NaCl, 1 mM DTT (pH 7.4) buffer. Spectra were acquired at 20 °C from 260 to 190 nm in continuous scanning mode with 0.5-nm steps, a bandwidth of 2 nm, and a scan speed of 50 nm/min. Five spectra per sample were accumulated and averaged to improve the signal to noise ratio. The appropriate solvent spectrum background was subtracted from each of these spectra.

ITC—ITC experiments were performed in PBS buffer (pH 7.4) at 25 °C using a MicroCal Auto iTC200 instrument (GE Healthcare). A 900 μM $YscU_C$ solution in the syringe was titrated against 90 μM YscI in the cell. The experiment involved 20 injections of 2 μl of the titrant protein ($YscU_C$) with 150 s between injections. The resulting raw data were fitted to a 1:1 binding model using the Origin 7.0 software package (GE Healthcare).

Pulldown of GST-tagged $YscU_C$ Variants with YscI—Proteins were produced as described above. GST-tagged YscU variants were resuspended in PBS buffer containing 1% Triton X-100, sonicated, and centrifuged for 20 min at 20,000 × *g* at 4 °C. The resulting supernatants were then incubated with a glutathione-Sepharose 4B slurry (GE Healthcare) for 1 h at 4 °C with gentle rocking. Bound proteins were washed with PBS containing 0.1% Triton X-100 and then used in an interaction assay. The YscI pellet was resuspended in PBS buffer containing 8 M urea, sonicated, and centrifuged for 20 min at 20,000 × *g* at 4 °C. The supernatant was then incubated with HIS-Select Nickel Affinity Gel (Sigma-Aldrich) for 1 h at 4 °C. Bound YscI was washed with PBS containing 0.1% Triton X-100 and eluted with 0.4 M imidazole in the same buffer. The GST-tagged YscU variants bound to the beads were incubated with 10 μM YscI for 3 h at 4 °C with gentle rocking. The beads were then washed with PBS containing 0.1% Triton X-100, and the proteins that remained bound to the beads were eluted using SDS-PAGE sample buffer and analyzed by immunoblotting.

Author Contributions—O. H., F. H. L., H. W.-W., and M. W.-W. designed experiments, analyzed data, and managed the project. O. H. and P. R. conducted experiments to characterize the domain structure of YscP. O. H. performed experiments to study the binding interface of YscP binding on YscU, YscP protection for the mutant P264A from autocleavage, and interaction of YscU and YscI by ITC. F. H. L. performed Yop and cytotoxicity assays for functional characterization of mutations at the YscU/YscP binding interface *in vivo* and GST binding assay for YscI to GST-tagged YscUC variants and discussed the project. T. E. performed secretion experiments. The manuscript was written by O. H., M. W.-W., F. H. L., and H. W.-W. All authors discussed the results and commented on the manuscript.

Acknowledgments—The NMR experiments were conducted at NMR4life, and we thank the Wallenberg and "Seth M. Kempes Minne" foundations for supporting this infrastructure. We acknowledge Dr. Stefan Frost, the Protein Expertise Platform (Umeå University, Sweden) and the Protein Science Facility (Karolinska Institute, Sweden) for assistance with protein cloning.

References

1. Portnoy, D. A., Wolf-Watz, H., Bolin, I., Beeder, A. B., and Falkow, S. (1984) Characterization of common virulence plasmids in *Yersinia* species and their role in the expression of outer membrane proteins. *Infect. Immun.* **43,** 108–114
2. Rosqvist, R., Forsberg, A., Rimpiläinen, M., Bergman, T., and Wolf-Watz, H. (1990) The cytotoxic protein YopE of *Yersinia* obstructs the primary host defence. *Mol. Microbiol.* **4,** 657–667
3. Hueck, C. J. (1998) Type III protein secretion systems in bacterial pathogens of animals and plants. *Microbiol. Mol. Biol. Rev.* **62,** 379–433
4. Ghosh, P. (2004) Process of protein transport by the type III secretion system. *Microbiol. Mol. Biol. Rev.* **68,** 771–795
5. Cornelis, G. R. (2006) The type III secretion injectisome. *Nat. Rev. Microbiol.* **4,** 811–825
6. Tampakaki, A. P., Fadouloglou, V. E., Gazi, A. D., Panopoulos, N. J., and Kokkinidis, M. (2004) Conserved features of type III secretion. *Cell. Microbiol.* **6,** 805–816
7. Yip, C. K., Kimbrough, T. G., Felise, H. B., Vuckovic, M., Thomas, N. A., Pfuetzner, R. A., Frey, E. A., Finlay, B. B., Miller, S. I., and Strynadka, N. C. (2005) Structural characterization of the molecular platform for type III secretion system assembly. *Nature* **435,** 702–707
8. Yip, C. K., and Strynadka, N. C. (2006) New structural insights into the bacterial type III secretion system. *Trends Biochem. Sci.* **31,** 223–230
9. Diepold, A., Wiesand, U., and Cornelis, G. R. (2011) The assembly of the export apparatus (YscR,S,T,U,V) of the *Yersinia* type III secretion apparatus occurs independently of other structural components and involves the formation of an YscV oligomer. *Mol. Microbiol.* **82,** 502–514
10. Edqvist, P. J., Olsson, J., Lavander, M., Sundberg, L., Forsberg, A., Wolf-Watz, H., and Lloyd, S. A. (2003) YscP and YscU regulate substrate specificity of the *Yersinia* type III secretion system. *J. Bacteriol.* **185,** 2259–2266
11. Agrain, C., Callebaut, I., Journet, L., Sorg, I., Paroz, C., Mota, L. J., and Cornelis, G. R. (2005) Characterization of a Type III secretion substrate specificity switch (T3S4) domain in YscP from *Yersinia enterocolitica*. *Mol. Microbiol.* **56,** 54–67
12. Macnab, R. M. (2003) How bacteria assemble flagella. *Annu. Rev. Microbiol.* **57,** 77–100
13. Minamino, T., and Macnab, R. M. (2000) Domain structure of *Salmonella* FlhB, a flagellar export component responsible for substrate specificity switching. *J. Bacteriol.* **182,** 4906–4914
14. Ferris, H. U., Furukawa, Y., Minamino, T., Kroetz, M. B., Kihara, M., Namba, K., and Macnab, R. M. (2005) FlhB regulates ordered export of flagellar components via autocleavage mechanism. *J. Biol. Chem.* **280,** 41236–41242
15. Makishima, S., Komoriya, K., Yamaguchi, S., and Aizawa, S.-I. (2001) Length of the flagellar hook and the capacity of the type III export apparatus. *Science* **291,** 2411–2413
16. Journet, L., Agrain, C., Broz, P., and Cornelis, G. R. (2003) The needle length of bacterial injectisomes is determined by a molecular ruler. *Science* **302,** 1757–1760
17. Mota, L. J., Journet, L., Sorg, I., Agrain, C., and Cornelis, G. R. (2005) Bacterial injectisomes: needle length does matter. *Science* **307,** 1278–1278
18. Büttner, D. (2012) Protein export according to schedule: architecture, assembly, and regulation of type III secretion systems from plant- and animal-pathogenic bacteria. *Microbiol. Mol. Biol. Rev.* **76,** 262–310
19. Agrain, C., Sorg, I., Paroz, C., and Cornelis, G. R. (2005) Secretion of YscP from *Yersinia enterocolitica* is essential to control the length of the injectisome needle but not to change the type III secretion substrate specificity. *Mol. Microbiol.* **57,** 1415–1427
20. Marlovits, T. C., Kubori, T., Lara-Tejero, M., Thomas, D., Unger, V. M., and Galán, J. E. (2006) Assembly of the inner rod determines needle length in the type III secretion injectisome. *Nature* **441,** 637–640
21. Mizuno, S., Amida, H., Kobayashi, N., Aizawa, S., and Tate S. (2011) The NMR structure of FliK, the trigger for the switch of substrate specificity in the flagellar type III secretion apparatus. *J. Mol. Biol.* **409,** 558–573
22. Bergeron, J. R., Fernández, L., Wasney, G. A., Vuckovic, M., Reffuveille, F., Hancock, R. E., and Strynadka, N. C. (2016) The structure of a type 3 secretion system (T3SS) ruler protein suggests a molecular mechanism for needle length sensing. *J. Biol. Chem.* **291,** 1676–1691
23. Sorg, I., Wagner, S., Amstutz, M., Müller, S. A., Broz, P., Lussi, Y., Engel, A., and Cornelis, G. R. (2007) YscU recognizes translocators as export substrates of the *Yersinia* injectisome. *EMBO J.* **26,** 3015–3024
24. Wiesand, U., Sorg, I., Amstutz, M., Wagner, S., van den Heuvel, J., Lührs, T., Cornelis, G. R., and Heinz, D. W. (2009) Structure of the type III secretion recognition protein YscU from *Yersinia enterocolitica*. *J. Mol. Biol.* **385,** 854–866
25. Lountos, G. T., Austin, B. P., Nallamsetty, S., and Waugh, D. S. (2009) Atomic resolution structure of the cytoplasmic domain of *Yersinia pestis* YscU, a regulatory switch involved in type III secretion. *Protein Sci.* **18,** 467–474
26. Weise, C. F., Login, F., H., Ho, O., Gröbner, G., Wolf-Watz, H., and Wolf-Watz, M. (2014) Negatively charged lipid membranes promote a disorder-order transition in the *Yersinia* YscU protein. *Biophys. J.* **107,** 1950–1961
27. Björnfot, A.-C., Lavander, M., Forsberg, A., and Wolf-Watz, H. (2009) Autoproteolysis of YscU of *Yersinia pseudotuberculosis* is important for regulation of expression and secretion of Yop proteins. *J. Bacteriol.* **191,** 4259–4267
28. Frost, S., Ho, O., Login, F. H., Weise, C. F., Wolf-Watz, H., and Wolf-Watz, M. (2012) Autoproteolysis and intramolecular dissociation of *Yersinia* YscU precedes secretion of its C-terminal polypeptide YscU(CC). *PLoS One* **7,** e49349
29. Login, F. H., and Wolf-Watz, H. (2015) YscU/FlhB of *Yersinia pseudotuberculosis* harbors a C-terminal type III secretion signal. *J. Biol. Chem.* **290,** 26282–26291
30. Kutsukake, K., Minamino, T., and Yokoseki, T. (1994) Isolation and characterization of FliK-independent flagellation mutants from *Salmonella typhimurium*. *J. Bacteriol.* **176,** 7625–7629
31. Williams, A. W., Yamaguchi, S., Togashi, F., Aizawa, S. I., Kawagishi, I., and Macnab, R. M. (1996) Mutations in fliK and flhB affecting flagellar hook and filament assembly in *Salmonella typhimurium*. *J. Bacteriol.* **178,** 2960–2970
32. Sukhan, A., Kubori, T., and Galán, J. E. (2003) Synthesis and localization of the *Salmonella* SPI-1 type III secretion needle complex proteins PrgI and PrgJ. *J. Bacteriol.* **185,** 3480–3483
33. Wood, S. E., Jin, J., and Lloyd, S. A. (2008) YscP and YscU switch the substrate specificity of the *Yersinia* type III secretion system by regulating export of the inner rod protein YscI. *J. Bacteriol.* **190,** 4252–4262
34. Diepold, A., Wiesand, U., Amstutz, M., and Cornelis, G. R. (2012) Assembly of the *Yersinia* injectisome: the missing pieces. *Mol. Microbiol.* **85,** 878–892
35. Sal-Man, N., Deng, W., and Finlay, B. B. (2012) EscI: a crucial component of the type III secretion system forms the inner rod structure in enteropathogenic *Escherichia coli*. *Biochem. J.* **442,** 119–125
36. Zhong, D., Lefebre, M., Kaur, K., McDowell, M. A., Gdowski, C., Jo, S., Wang, Y., Benedict, S. H., Lea, S. M., Galan, J. E., and De Guzman, R. N. (2012) The *Salmonella* type III secretion system inner rod protein PrgJ is partially folded. *J. Biol. Chem.* **287,** 25303–25311
37. Lefebre, M. D., and Galán, J. E. (2014) The inner rod protein controls substrate switching and needle length in a *Salmonella* type III secretion system. *Proc. Natl. Acad. Sci. U.S.A.* **111,** 817–822
38. Galán, J. E., and Wolf-Watz, H. (2006) Protein delivery into eukaryotic cells by type III secretion machines. *Nature* **444,** 567–573
39. Rosqvist, R., Magnusson, K. E., and Wolf-Watz, H. (1994) Target cell contact triggers expression and polarized transfer of *Yersinia* YopE cytotoxin into mammalian cells. *EMBO J.* **13,** 964–972

40. Botteaux, A., Sani, M., Kayath, C. A., Boekema, E. J., and Allaoui, A. (2008) Spa32 interaction with the inner-membrane Spa40 component of the type III secretion system of *Shigella flexneri* is required for the control of the needle length by a molecular tape measure mechanism. *Mol. Microbiol.* **70,** 1515–1528
41. Stainier, I., Bleves, S., Josenhans, C., Karmani, L., Kerbourch, C., Lambermont, I., Tötemeyer, S., Boyd, A., and Cornelis, G. R. (2000) YscP, a *Yersinia* protein required for Yop secretion that is surface exposed, and released in low Ca^{2+}. *Mol. Microbiol.* **37,** 1005–1018
42. Monjarás Feria, J. V., Lefebre, M. D., Stierhof, Y.-D., Galán, J. E., and Wagner, S. (2015) Role of autocleavage in the function of a type III secretion specificity switch protein in *Salmonella enterica* serovar Typhimurium. *mBio* **6,** e01459-01415
43. Radics, J., Königsmaier, L., and Marlovits, T. C. (2014) Structure of a pathogenic type 3 secretion system in action. *Nat. Struct. Mol. Biol.* **21,** 82–87
44. Schneider, C. A., Rasband, W. S., and Eliceiri, K. W. (2012) NIH Image to ImageJ: 25 years of image analysis. *Nat. Methods* **9,** 671–675
45. Akopyan, K., Edgren, T., Wang-Edgren, H., Rosqvist, R., Fahlgren, A., Wolf-Watz, H., and Fallman, M. (2011) Translocation of surface-localized effectors in type III secretion. *Proc. Natl. Acad. Sci. U.S.A.* **108,** 1639–1644
46. Delaglio, F., Grzesiek, S., Vuister, G. W., Zhu, G., Pfeifer, J., and Bax, A. (1995) NMRPipe: a multidimensional spectral processing system based on UNIX pipes. *J. Biomol. NMR* **6,** 277–293
47. Helgstrand, M., Kraulis, P., Allard, P., and Härd, T. (2000) Ansig for Windows: an interactive computer program for semiautomatic assignment of protein NMR spectra. *J. Biomol. NMR* **18,** 329–336
48. Williamson, M. P. (2013) Using chemical shift perturbation to characterise ligand binding. *Prog. Nucl. Magn. Reson. Spectrosc.* **73,** 1–16